NDT&E International 143 (2024) 103034

Contents lists available at ScienceDirect

NDT and E International

journal homepage: www.elsevier.com/locate/ndteint

Non-destructive estimation of mechanical properties in Usibor® 1500 via thermal diffusivity measurements: A thermographic procedure

G. Dell'Avvocato [a,*], P. Bison [b], M.E. Palmieri [a], G. Ferrarini [b], D. Palumbo [a], L. Tricarico [a], U. Galietti [a]

[a] Department of Mechanics, Mathematics and Management, Polytechnic University of Bari, Via Orabona 4, 70125, Bari, Italy
[b] Institute of Construction Technologies (CNR-ITC), National Research Council of Italy, 35127, Padua, Italy

ARTICLE INFO

Keywords:
Infrared thermography
Ultimate tensile strength
Laser thermography
Boron steel
Microstructure
Thermal diffusivity

ABSTRACT

The study investigated the anti-correlation between thermal diffusivity and Ultimate Tensile Strength (UTS) in Usibor® 1500 steel. The non-destructive pulsed laser spot thermography technique was used to analyze fifteen boron steel specimens with varying bainite/martensite phase percentages, while the UTS was measured through uniaxial tensile tests. A 23 % thermal diffusivity difference was found between fully martensitic and fully bainitic structures, with UTS varying by around 90 %. The strong anti-correlation was confirmed (Spearman coefficient −0.98) and an empirical power-law equation was derived to estimate UTS based on thermal diffusivity variations. The approach showed an R-squared value over 0.84, providing a non-destructive thermographic procedure for UTS estimation in Usibor® 1500 steel, offering valuable material property insights.

1. Introduction

In the industrial sector, a crucial requirement is to tailor the mechanical properties of components to suit specific applications. For metallic materials, thermal treatments, including the widely used tempering process, play a vital role in achieving these objectives. An example of heat treatment is the press hardening process used with tailored technologies to achieve automotive structural components with high mechanical strength in one area and high ductility in another, as seen in the car's central pillar (B-Pillar) [1,2] This component needs to both prevent intrusions and absorb energy during impacts.

Traditionally, verifying the successful outcome of thermal treatment, i.e., the desired microstructure variation, has involved destructive testing, such as tensile tests or metallography, or semi-destructive methods, like hardness tests. However, these tests inevitably alter the surface of the component, compromising mechanical strength, particularly in structural applications. Furthermore, they are costly, time-consuming, and poorly suited for industrial applications.

To overcome these limitations, non-destructive testing (NDT) techniques offer an intriguing alternative. Among these, thermographic testing stands out as a promising approach, with applications including process control [3–5], defect detection [6–14], and mechanical [15–18] and thermophysical characterisation [19–31]. Stimulated thermography offers full-field, non-contact evaluations without surface preparation and significantly reduces testing time compared to traditional methods.

The literature has demonstrated an "anti-correlation" between thermal diffusivity in metals and hardness, providing a basis for this study's approach [20,32–35]. Non-destructive thermographic measurements of thermal diffusivity were employed to establish an empirical relationship enabling the estimation of mechanical properties, specifically the Ultimate Tensile Strength (UTS) of the Usibor®1500 boron steel.

Thermal diffusivity measurements using thermographic methods are well-established and widely adopted, with various applicable techniques [19–28,31,36–40]. Over the years, researchers have introduced laser flash methods [19,27,41], spatial flash sources [42,43], and moving laser sources [23,25,44] for thermal diffusivity measurements. Among these, pulsed laser spot thermography [26,30,31,45] is a preferred method due to its simplicity, robustness, and suitability for future industrial applications.

Previous works have evaluated the proposed methodology's ability to distinguish qualitatively between different microstructures and studied the influence of experimental test parameters on surface thermal diffusivity measurements [46–48]. This led to the development of a procedure for selecting optimal experimental parameters [46] for the in-plane thermal diffusivity measurement. Additionally, an initial

* Corresponding author.
E-mail address: giuseppe.dellavvocato@poliba.it (G. Dell'Avvocato).

https://doi.org/10.1016/j.ndteint.2023.103034
Received 29 August 2023; Received in revised form 1 December 2023; Accepted 27 December 2023
Available online 30 December 2023

attempt was made to correlate thermal diffusivity with UTS [47] considering a fully martensitic structure and a ferritic-pearlitic ones.

In the previous work [47], where a non-destructive thermographic procedure was proposed for a qualitative assessment of surface heat treatment, focusing on ferritic-pearlitic and martensitic structures, further advancements have been made. Specifically, the bainitic and martensitic phases were considered, including intermediate levels of percentage composition. Mechanical tests were conducted to develop a quantitative, non-destructive thermographic procedure for estimating the Ultimate Tensile Strength (UTS) in boron steels.

In particular, this study presents a comprehensive quantitative test procedure for measuring in-depth thermal diffusivity using pulsed laser spot thermography. Subsequently, an extensive experimental campaign established an anti-correlation between the measured thermal diffusivity values and the ultimate tensile strength. This pioneering application of thermography as a non-destructive method allows for estimating the Ultimate Tensile Strength (UTS) in the boron steel Usibor® 1500 and determining the percentages of microstructures present. Furthermore, we assessed the influence of a protective Al–Si coating on thermal diffusivity measurements and proposed a relationship that accounts for the presence of this coating. These aspects constitute the main advancements compared to the previous works [46–48].

2. Theory

As already mentioned in the introductive section, among the plethora of possible methods for thermal diffusivity measurement [19–28,31,36–40,45–47], the one employed in this research work is the pulsed laser spot thermography [22,31,45,47], a well-established technique widely documented in the literature. This method is based on the model of temperature variation in both the in-plane and along the material thickness after applying a Dirac pulse heating using a laser with a spot radius R, on a finite body of thickness L, as shown below.

$$T(x,y,0,t)=\frac{2Q_0}{\pi}\frac{e^{-\frac{x^2+y^2}{\sigma_t^2}}}{\sigma_t^2}\left[\frac{1}{\rho CL}\left(1+2\sum_{n=1}^{\infty}e^{-\frac{n^2\pi^2\alpha_n t}{L^2}}\right)\right] \quad (1)$$

In the above equation, T represents the temperature distribution as function of time t, α_n represents the thermal diffusivity of the material in the z direction, σ_t is related to the evolution of temperature distribution on the surface in time, thus to the in-plane thermal diffusivity, C represents the specific heat, and ρ represents the material density. This equation can be separated into two factors, where one exclusively contains terms related to in-plane diffusion and the other solely contains terms related to diffusion along the thickness. In this study, after verifying through previous experiments that the material can be considered isotropic, we solely evaluated the thermal diffusivity along the thickness. This approach was primarily adopted due to the limited available area on the specimen, which will be discussed in the next sections, aiming to avoid the influence of edges on the measurement of in-plane thermal diffusivity.

3. Material and methods

3.1. Specimens

In order to obtain samples with a different percentage of bainitic and martensitic microstructural phases, the methodology described by Palmieri et al. [49] was adopted. Below is a summary of this methodology.

First, using an automotive B-Pillar as a case study, the press hardening process with the tailored tool tempering approach was numerically simulated. This process differentiates tool temperatures, specifically a portion of the tools is heated, and another portion is cooled [50]. As a result, during the quenching phase, the blank in contact with the hot tools cools slowly, leading to a bainitic microstructure, while the blank in contact with the cold tools cools rapidly, creating a martensitic microstructure. With this approach, a transition zone is formed between the two different regions, exhibiting a gradual variation in microstructure from fully bainitic to fully martensitic.

The numerical model enabled the estimation of thermal cycles and corresponding percentages of microstructural phases at five points within the transition zone. Fig. 1 illustrates the thermal cycles at these points, and Table 1 presents the corresponding percentages of martensitic and bainitic phases.

The thermal cycles acquired in these five points were finally reproduced on samples in 22MnB5 (USIBOR®1500P). These experimental tests were conducted using the Gleeble®3180 physical simulator, which is a system capable of reproducing thermal and/or thermo-mechanical manufacturing processes on a laboratory scale.

For each condition, three physical simulation tests were conducted with the aim of ensuring statistical significance. The geometry of the samples adopted for this study is shown in Fig. 2a. The thickness of the samples is 1.1 ± 0.08 mm.

To replicate the thermal cycles, the Gleeble physical simulator employs the Joule effect. The specimen is held between two copper grips, allowing for the passage of current. These grips are then placed inside two jaws cooled by means of a water-glycol solution. The experimental setup is shown in Fig. 2 b.

A K-type thermocouple was welded onto the specimen centre (Fig. 2a.), serving as a pilot thermocouple. Inside the system, there is a PID controller which modulates the current density to ensure that the temperature at the control point matches the set temperature. During a physical simulation test, a thermal gradient is produced along the specimen, with the set temperature at the centre and decreasing as it approaches the cold grips.

The geometry of the sample ensures a thermal gradient during the test of about 8 K/mm, guaranteeing that within 5 mm from the centre of the sample, the microstructure estimated by the numerical model is obtained for each considered thermal cycle. The total width in which there is uniformity of microstructure is approximately 10 mm.

The microstructure's uniformity throughout the specimen volume in the central area of the specimens was thoroughly verified, making us consider it isotropic within the region of interest. For example, Fig. 3 shows the microstructures obtained at the centre of the sample subjected to the thermal cycle of point A (Fig. 3a) and the thermal cycle of point C (Fig. 3b). As expected, a predominantly bainitic microstructure is obtained during the thermal cycle at point A, while a predominantly

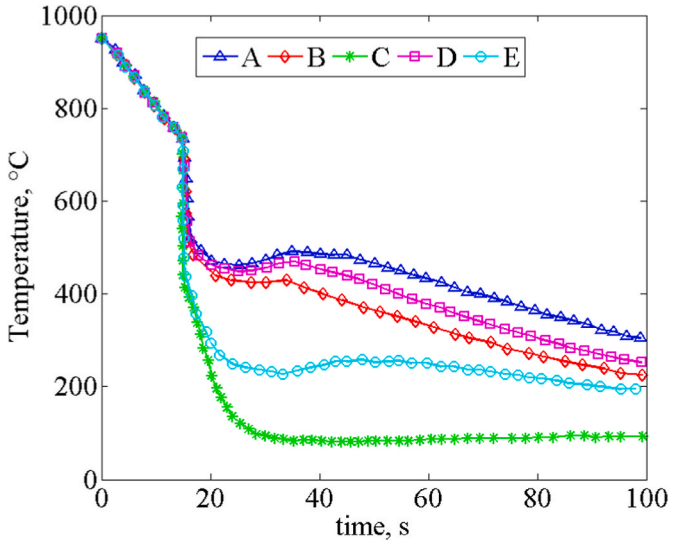

Fig. 1. Thermal cycles acquired from numerical model in the five points along the transition zone.

Table 1
Percentage of martensitic and bainitic microstructural phases in the five points.

Points	Martensitic phase [%]	Bainitic phase [%]
A	0	100
B	56	44
C	100	0
D	15	85
E	82	18

martensitic microstructure is obtained during the thermal cycle at point C.

The thickness measurements obtained for each specimen are presented in Table 2. The measurements were performed using a micrometre; each repeated five times on each specimen. This approach is essential because the proposed method's thermal diffusivity measurement is susceptible to accurately determining the specimen's thickness. Therefore, the thickness needs to be precisely known and carefully measured. The Usibor® 1500 sheets under investigation arrive with a coating, about 50 μm thick, comprising a ternary alloy layer at the steel-coating interface and a binary Al–Si alloy layer. Following the quenching process, the Al–Si coating undergoes transformations in the furnace, involving interdiffusion and solidification reactions, resulting in several protective intermetallic layers composed of Al–Fe–Si alloy. This coating is pivotal in measuring thermal diffusivity, mainly when conducting measurements along the material's thickness. Given the distinct thermophysical properties of the coating relative to the underlying steel, it can significantly influence the absolute determination of thermal diffusivity. Therefore, to mitigate this effect, we adopted a prudent approach where, for each specimen, the coating layer was mechanically removed from one of the two lateral surfaces using abrasive paper.

This approach enables us to conduct measurements on both sides of each specimen, with the only variable being the presence or absence of the Al–Si coating. By doing so, we can effectively isolate and assess the impact of the coating layer on the thermal diffusivity measurements, thereby ensuring a more precise and accurate evaluation of the material's properties.

Table 2
Geometrical dimensions and characteristics of investigated specimens.

ID	Martensite [%]	Bainite [%]	Thickness
A 01	0	100	1.15 ± 0.01 mm
A 02	0	100	1.12 ± 0.01 mm
A 01	0	100	1.10 ± 0.02 mm
B 01	56	44	1.07 ± 0.01 mm
B 02	56	44	1.06 ± 0.01 mm
B 03	56	44	1.05 ± 0.01 mm
C 01	100	0	1.04 ± 0.01 mm
C 02	100	0	1.05 ± 0.01 mm
C 03	100	0	1.04 ± 0.01 mm
D 01	15	85	1.04 ± 0.01 mm
D 02	15	85	1.04 ± 0.01 mm
D 03	15	85	1.05 ± 0.01 mm
E 01	82	18	1.07 ± 0.01 mm
E 02	82	18	1.06 ± 0.01 mm
E 03	82	18	1.08 ± 0.01 mm

3.2. Experimental setup

The central part of the specimen described before was heated using a 1064 nm NdYag laser source with a circular spot and a top-hat distribution for a time of 300 μs with a nominal energy of 3.75 J. The laser operates continuously (CW) during the 300 μs period of pump lamp ignition, which can be approximated as a pulse for the specific model under consideration. This approximation has no significant impact on the measurement. As mentioned, the nominal microstructure occurs only in the central area of the specimens. Thus, it is crucial that the laser

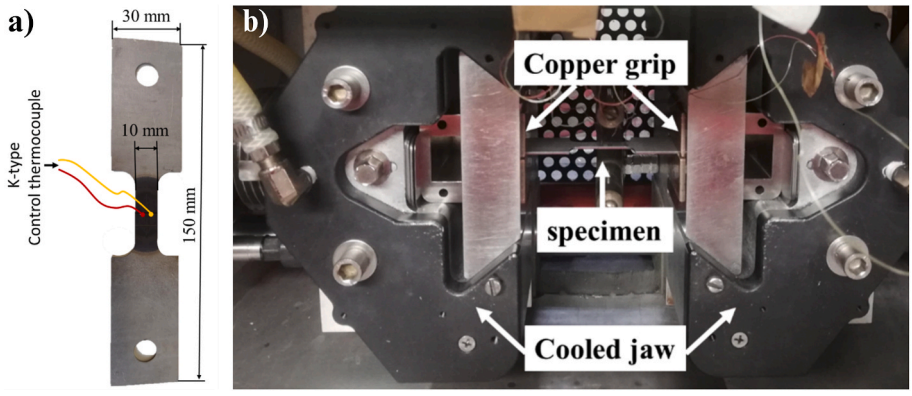

Fig. 2(a). Specimen used for physical simulation tests and (b) Set-up adopted for the physical simulation tests.

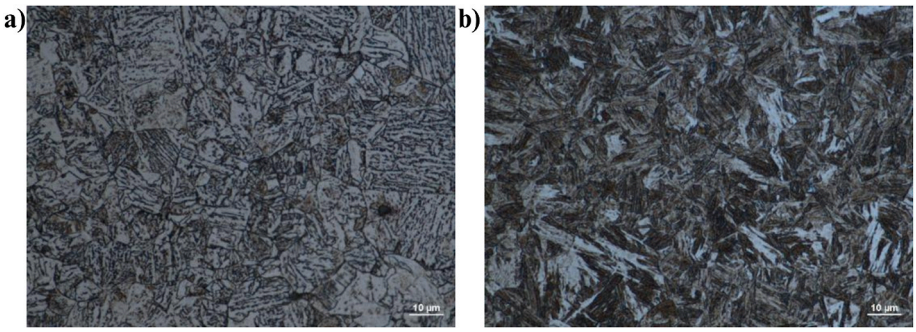

Fig. 3. (a) Bainitic microstructure at the centre of the samples subjected to the thermal cycle of point A and **(b)** Martensitic microstructure at the centre of the samples subjected to the thermal cycle of point C.

spot, therefore the inspected area, is entirely within the area highlighted in Fig. 4. To reduce the spot size to the desired dimension, a lens was employed coaxially with the laser beam, resulting in a spot diameter of d~6.6 mm. The heating and cooling phases have been recorded by a cooled IR detector FLIR series 6000 in a one-side setup, as shown in Fig. 5 and schematized in Fig. 5 b. For each test, a thermal sequence with a duration of *2.5s* has been recorded with an acquisition frequency of 1 kHz, a spatial resolution of *0.*278 mm*/pixel* and a calibration interval *-10 C* to *55°C*. In Fig. 5 c-d the details of inspected surfaces are shown to highlight the difference between the coated surface and the non-coated ones.

To avoid distortions, the specimens were positioned with a surface inclined at an angle of 15° relative to the laser beam (Fig. 5b) and facing the thermal camera after verifying that the slight beam inclination did not affect the diffusivity measurement [47].

After these tests for thermal diffusivity analysis, the samples were subjected to tensile tests to assess their mechanical properties in terms of Ultimate Tensile Strength (UTS).

The tensile tests were performed using the INSTRON 4485 universal testing machine controlled by Zwick-Roell software, with a crosshead speed set at 10 mm/min. The experimental setup is shown in Fig. 6a.

Before the tensile tests, the specimens were machined to achieve the geometry shown in Fig. 6 b. A notch was created at the centre of the specimen to localize the deformation at this specific point, which was subjected to the thermal cycle set during the physical simulation test. Moving far from the specimen centre, the thermal cycles vary due to the thermal gradient generated during the physical simulation test, as described in section 3.1. Therefore, the notch was essential to characterize the mechanical properties corresponding to the microstructure obtained under the specific thermal cycle.

3.3. Methods

In order to validate the accuracy of the thermographic method for measuring thermal diffusivity, preliminary tests were carried out on specimens with a 100 % martensitic structure. Before conducting the thermographic measurements, these specimens underwent testing using the well-established Transient Plane Source method [51]. By conducting these tests, the capability of the thermographic method to provide consistent results with standard methods was confirmed.

As described in the preceding section, the initial sheet material is coated with a thin Al–Si layer, which is a protective coating during post-production processes. However, due to the contrasting thermophysical properties of Al–Si compared to boron steel, this layer has the potential to affect the measurement of thermal diffusivity. Although the layer's thickness is negligible in relation to the overall sheet thickness, it is necessary to consider its influence.

To account for this factor and assess its impact on thermal diffusivity measurements, manual removal of the Al–Si layer was performed on one of the specimen's faces before the thermographic analysis. This approach ensured that tests could be conducted on both surfaces within the same localized region. Each specimen underwent five repetitions of thermal diffusivity measurements on each side, resulting in a comprehensive total of ten measurements per specimen across the entirety of the fifteen specimens, Consequently, this yielded seventy-five measurements for the coated side and an equivalent seventy-five measurements for the uncoated side.

For each thermographic test, an inspection area of 36 x 36 *pixels* was analysed, with the centre coinciding with the laser spot and the centre of the specimen itself (Fig. 7). Therefore, the signal corresponding to the area of interest was detected and analysed for each test over a total duration of 0.270 s. Subsequently, a fitting operation was performed using the previously mentioned relationship, resulting in the value α/L^2 where α is the thermal diffusivity through the thickness and L the thickness of the metal plate considered (Fig. 7c). By multiplying this value with the squared thickness of the specimen used in the test, the thermal diffusivity along the thickness within the inspected region was determined. This procedure was applied to each specimen, both for the surface covered by the protective coating and the surface where it was removed. As a result, two average thermal diffusivity values were obtained for each specimen, one corresponding to the side with the coating and the other to the side without it.

Following the thermographic analysis, uniaxial tensile tests were performed on the identical specimens to determine their ultimate tensile strength.

The results of the thermographic tests were compared with the data obtained from the tensile tests to establish a correlation between thermal diffusivity and ultimate tensile strength. This correlation was evaluated for both cases: with and without the presence of the Al–Si layer, to assess its impact on the relationship. Each step of the proposed procedure is summarized in Fig. 8.

Based on the observed data, empirical relationships were derived in

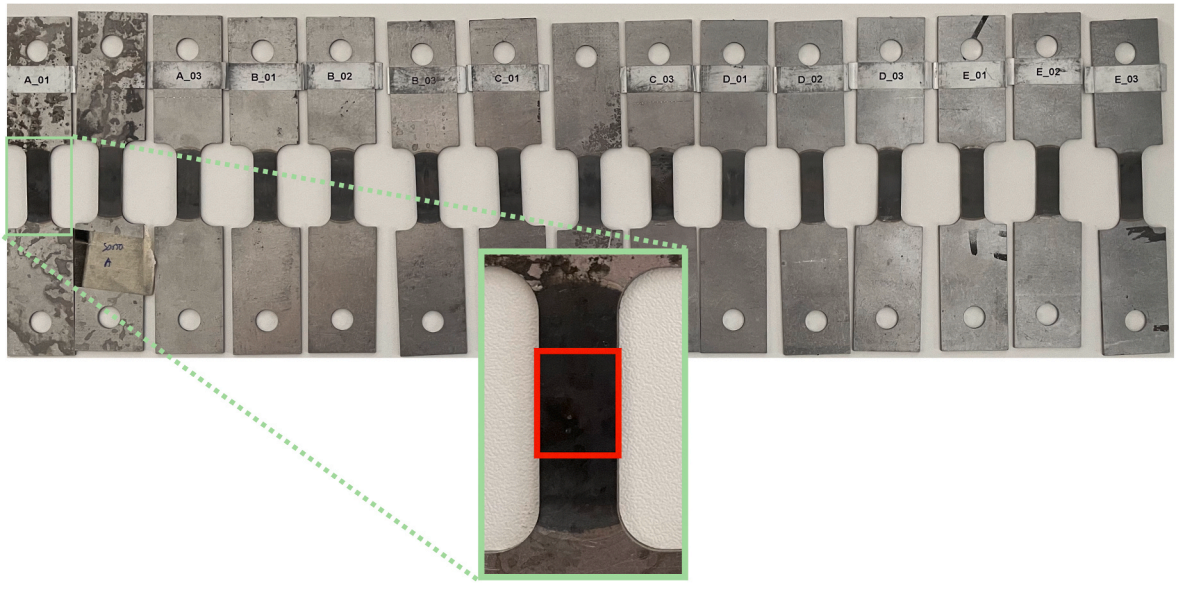

Fig. 4. Above are the inspected specimens. The IDs correspond to the properties summarized in the table below. The magnification highlights the area of interest of the specimen where the structure matches the nominal one.

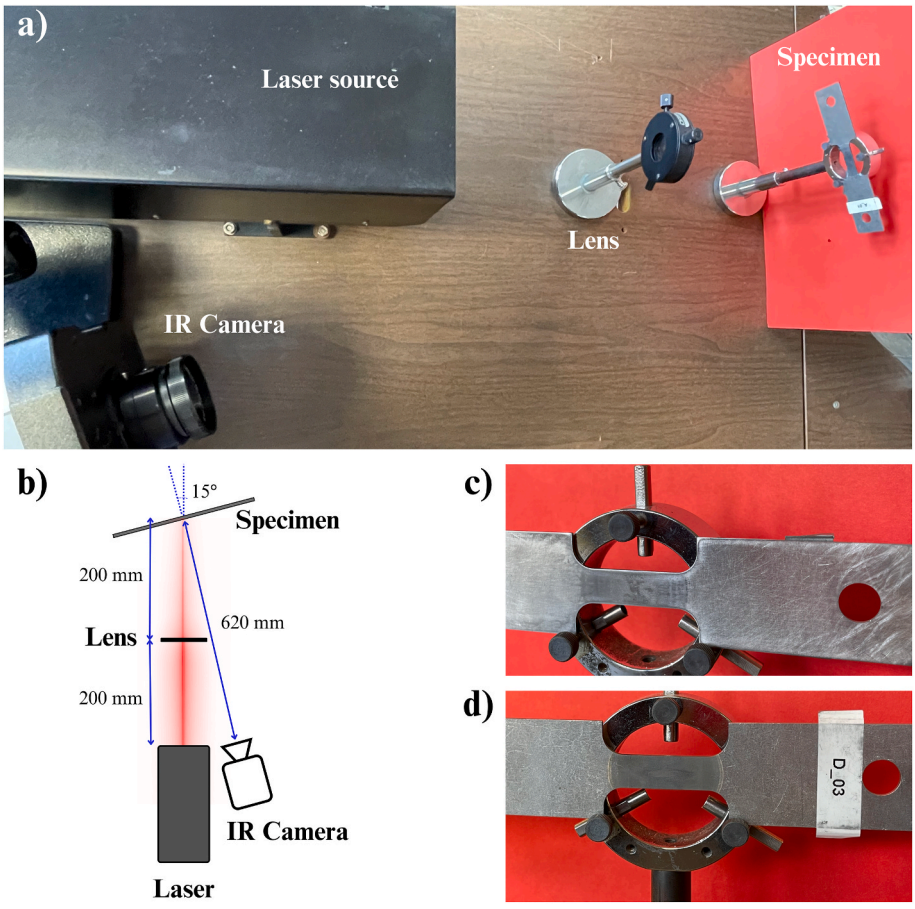

Fig. 5. The experimental thermographic setup was adopted for thermal diffusivity measurements using the pulsed laser spot method. a) An overview of the setup with the instrumentation used. b) An explanatory diagram of the setup in reflection mode. c-d) Details of the inspected area during the tests: (c) without the protective coating, and (d) with the coating from the opposite side of the same specimen.

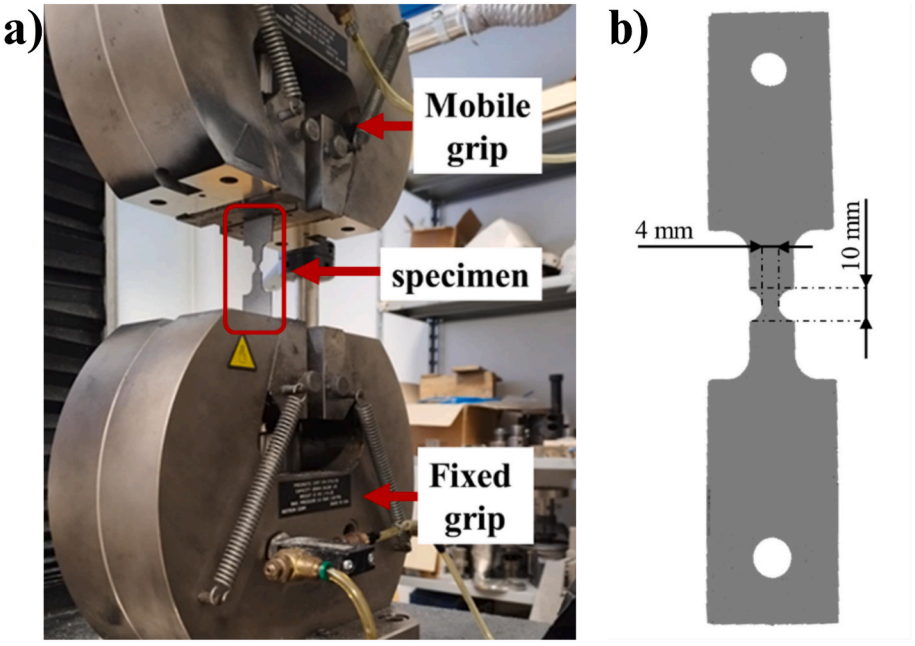

Fig. 6. (a) Experimental setup for the tensile tests and (b) Geometry of the specimen used for the tensile tests (notched sample).

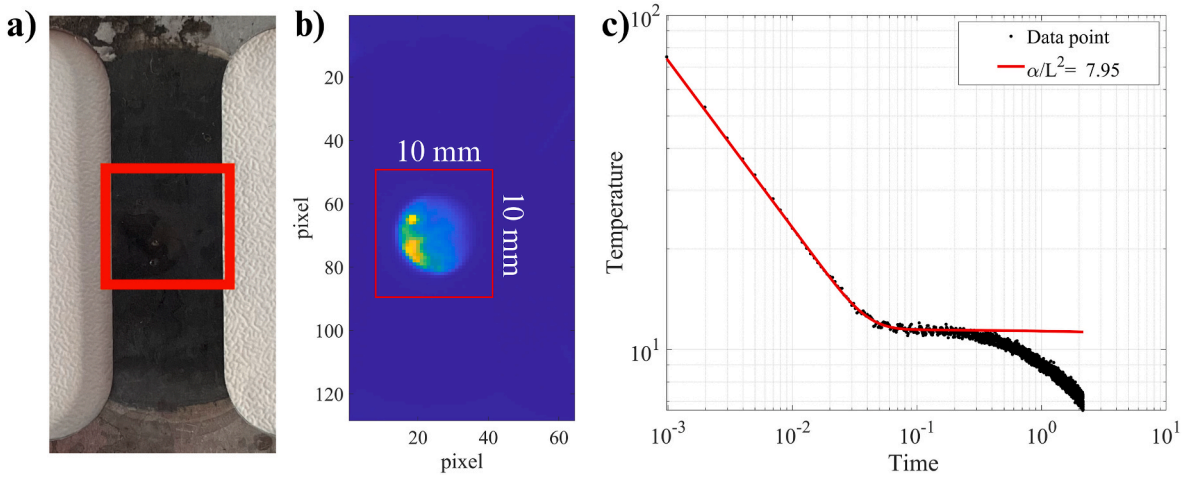

Fig. 7. a) Detail of one of the analysed specimens with the inspected area highlighted. **b)** Exemplary thermogram showing the laser spot imprint and the area considered for applying the method for thermal diffusivity measurement. **c)**Experimental data from the test shown, depicting the temperature evolution over the experimental time (black dots), along with the regression curve obtained by applying the model (red line). (For interpretation of the references to colour in this figure legend, the reader is referred to the Web version of this article.)

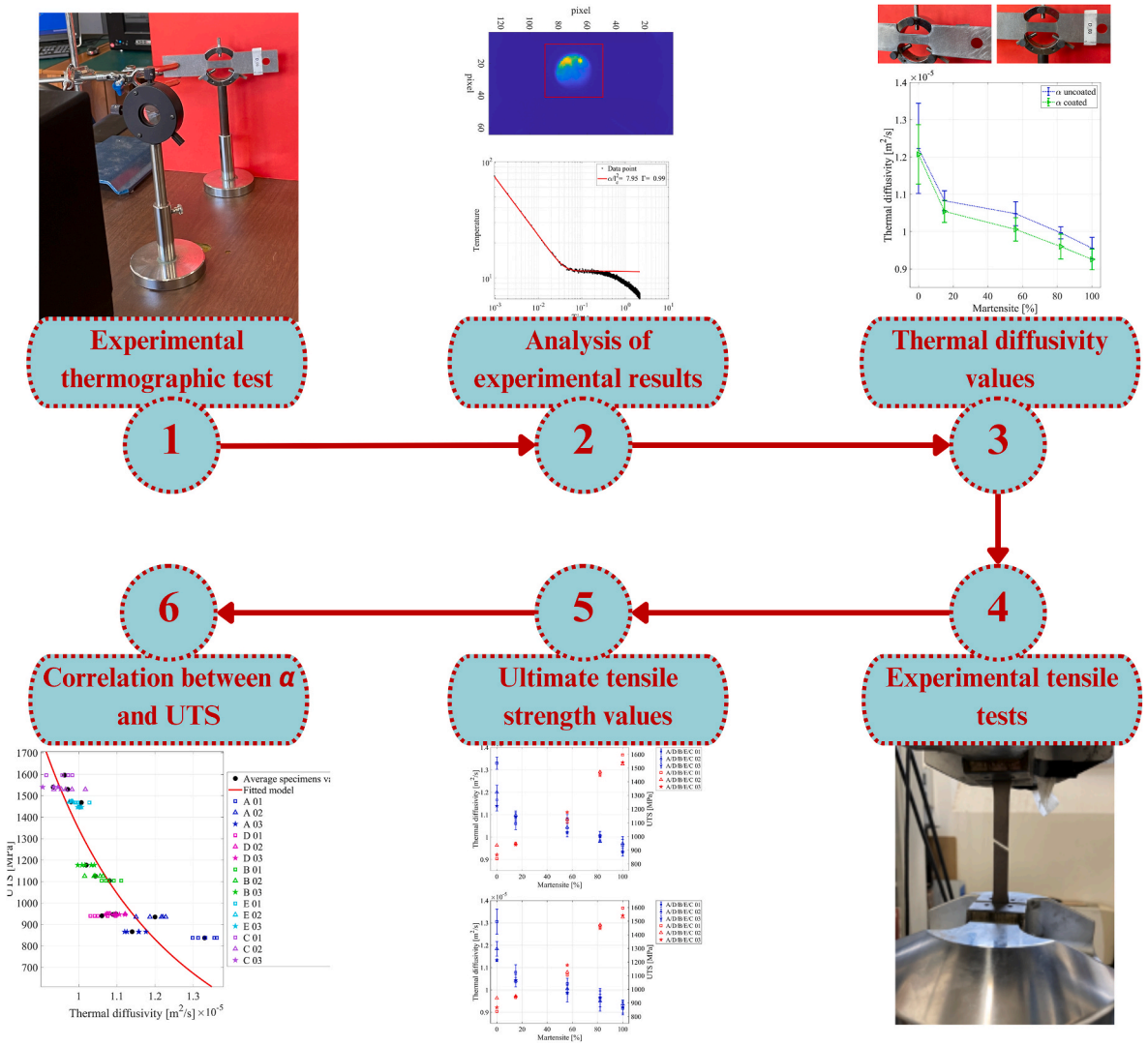

Fig. 8. A graphical summary of the procedure used in the current research work.

both scenarios to estimate the material's ultimate tensile strength, given the known thermal diffusivity. These empirical relationships provide a practical way to predict the ultimate tensile strength using the measured thermal diffusivity as a parameter.

4. Results

Table 3 displays the thermal diffusivity values obtained from the thermographic tests, both with and without the coating. The diffusivity values for each specimen were determined by averaging the results of five repetitions. Subsequently, the mean value for each nominal phase percentage was calculated by averaging the results from three replicates, along with their respective 95 % confidence intervals.

The thermal diffusivity value obtained for the 100 % martensitic microstructure aligns with the results from the TPS tests, indicating a difference between the two measurements is approximately 8 %. It is important to note that the thermal diffusivity value obtained in the presence of the coating was used as a reference, as the TPS tests were conducted without removing the layer. Hence, the presence of the coating should be taken into consideration when comparing the results.

Fig. 9 depicts the thermal diffusivity values plotted against the nominal microstructure percentages for each phase composition, along with their corresponding uncertainty bands which is considered across the fifteen measurements: five repetitions of the measurement for each of the three specimen replications. Additionally, the results obtained without the Al–Si coating are highlighted in blue.

In Fig. 10, the graphs illustrating the thermal diffusivity values and ultimate tensile strength (UTS) are plotted against the nominal microstructural phase percentages.

In Fig. 11, we have plotted the ultimate tensile strength (UTS) against thermal diffusivity for both coated and uncoated cases. Each colour corresponds to a distinct microstructure, representing different percentages of bainite and martensite, whereas the black data points indicate the average values for each specimen. The red curve represents the model used for estimating UTS based on thermal diffusivity.

5. Discussion

The comparison between the thermal diffusivity measurements obtained through the thermographic technique and TPS reveals an exceedingly small difference around 8 %. This finding unequivocally confirms the accuracy of the thermographic method for assessing thermal diffusivity.

It is noteworthy that, for each nominal phase percentage, the average values from the three replicated tests exhibit a certain level of dispersion. This dispersion contributes to the widening of the confidence interval associated with the measurement of the diffusivity obtained from the three specimens with the same nominal phase percentage.

The results depicted in Fig. 9 demonstrate a consistent trend: all the diffusivity values obtained from the tests conducted without the Al–Si coating are higher compared to those measured in the presence of the coating. This behaviour can be attributed to the distinctive thermophysical properties inherent to the Al–Si coating. Plausibly, the coating possesses a lower thermal diffusivity value than the steel substrate. Consequently, its presence influences the overall measured diffusivity within the material's thickness, resulting in an intermediate diffusivity value between the diffusivity of the coating and that of the steel substrate. This phenomenon highlights the significance of considering coatings' thermal properties when assessing layered materials' thermal diffusivity. The evaluation also considers that the differences between the thermal diffusivity values obtained with and without coating may exhibit minor variations and are not constant. This variation in behaviour can be attributed to the manual coating removal process, which introduces potential inconsistencies in the amount of coating removed from each specimen. As it was manually done using sandpaper, the complete coating removal might not be uniform across all specimens yet. Consequently, the presence of any residual coating layer could lead to variations in its thickness among the specimens. These differences were not initially present in the supplied state but emerged during the manual removal. On the contrary, concerning the results obtained from the coated specimens, although the presence of the coating undoubtedly exerts a more substantial influence on the absolute measurement of diffusivity, the coating layer can be considered identical for all specimens since it remains the same as the one provided with the sheet metal.

Moreover, it is worth noting the considerable extent of the uncertainty intervals for each nominal phase percentage. However, upon closer examination of Fig. 10, it becomes apparent that the individual specimen uncertainties are relatively small with an average standard deviation value of 2 %. The widening of the overall uncertainty interval primarily stems from replicating tests across multiple specimens. This suggests that the variation in diffusivity values among the specimens primarily reflects microstructural non-uniformity induced by the adopted heat treatment process rather than inherent measurement uncertainty.

Conversely, this underscores the remarkable sensitivity of diffusivity to microstructural variations, surpassing that of ultimate tensile strength (UTS) measurements. These results were expected since UTS provides macro information about the microstructure with respect to the local analysis provided by the proposed approach. Moreover, these findings emphasize the paramount importance of diffusivity as a critical parameter for characterizing material behaviour, as even minor changes in microstructure can significantly impact diffusivity values.

By conducting a Spearman correlation analysis to investigate the relationship between thermal diffusivity and ultimate tensile strength (UTS), we obtained a strong anti-correlation with a coefficient of approximately −0.98 for both coated and uncoated samples. This means

Table 3
Summary table of the results obtained for each specimen concerning thermal diffusivity with and without coating and ultimate tensile strength.

ID	Martensite [%]	Repetitions	Thermal diffusivity (Coated) [mm^2/s]	Thermal diffusivity (Uncoated) [mm^2/s]	Ultimate tensile strength [MPa]
A 01	0	5	13.06 ± 0.04	13.33 ± 0.03	838
A 02	0	5	11.84 ± 0.03	12.00 ± 0.03	935
A 01	0	5	11.33 ± 0.01	11.48 ± 0.02	866
B 01	56	5	10.28 ± 0.02	10.83 ± 0.02	1104
B 02	56	5	10.05 ± 0.01	10.44 ± 0.02	1125
B 03	56	5	9.86 ± 0.04	10.19 ± 0.02	1177
C 01	100	5	9.18 ± 0.03	9.60 ± 0.03	1596
C 02	100	5	9.36 ± 0.02	19.71 ± 0.03	1529
C 03	100	5	9.23 ± 0.03	9.33 ± 0.02	1540
D 01	15	5	10.78 ± 0.03	10.59 ± 0.03	940
D 02	15	5	10.41 ± 0.03	10.91 ± 0.02	949
D 03	15	5	10.44 ± 0.02	10.98 ± 0.02	947
E 01	82	5	9.65 ± 0.02	10.07 ± 0.02	1468
E 02	82	5	9.50 ± 0.04	9.80 ± 0.01	1471
E 03	82	5	9.65 ± 0.04	10.03 ± 0.01	1447

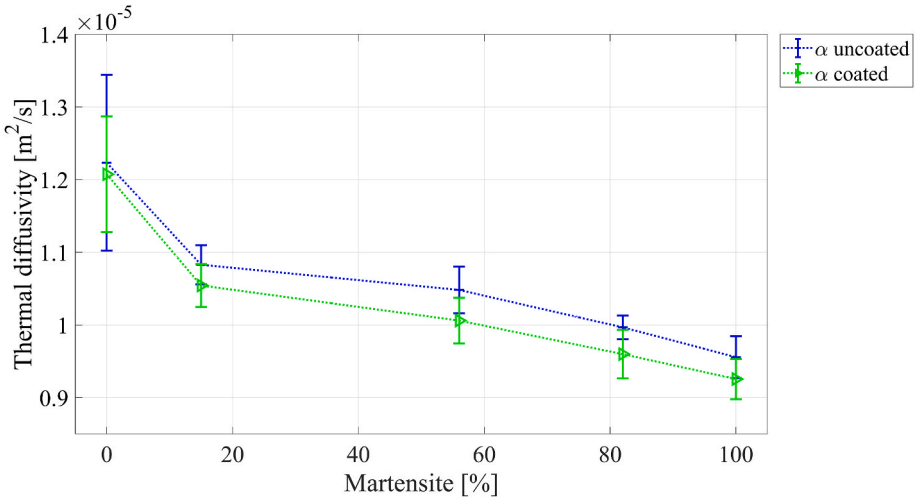

Fig. 9. The average thermal diffusivity values were obtained for each investigated phase percentage. In green are the values obtained from measurements carried out on the coated side, while in blue are those obtained from the side where the coating was removed. Error bars represent the standard deviation across the fifteen measurements: five repetitions of the measurement for each of the three specimen replications. (For interpretation of the references to colour in this figure legend, the reader is referred to the Web version of this article.)

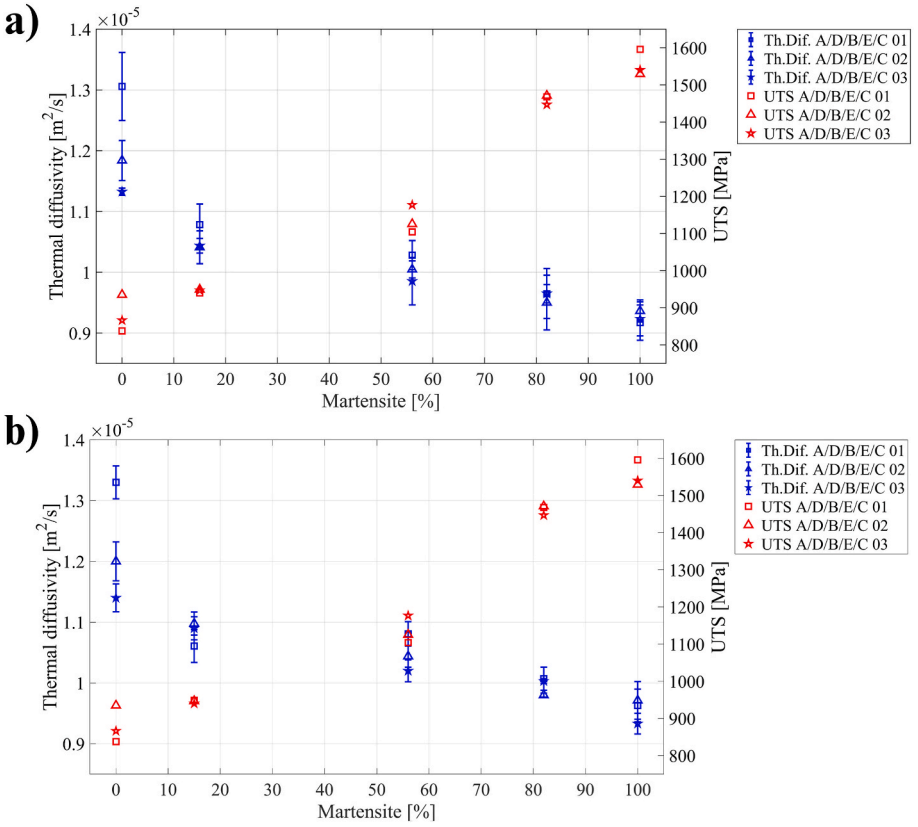

Fig. 10. The blue dots are values of thermal diffusivity The red points represent each specimen's Ultimate Tensile Strength (UTS) values. The thermal diffusivity values for each specimen obtained (a) without coating and (b) with coating. Error bars represent the standard deviation among the five repetitions for each specimen. (For interpretation of the references to colour in this figure legend, the reader is referred to the Web version of this article.)

a clear connection between these material properties is present. We employed a power-law regression model to establish the relationship quantitatively, which demonstrated a commendable fit with R^2 values of about 0.82 for coated samples and 0.84 for uncoated ones.

Upon examining Fig. 11, illustrating the correlation between UTS and thermal diffusivity for both coated and uncoated scenarios, we noticed some critical aspects concerning the proposed model intended for UTS estimation. Specifically, the region within the 10–10.5 mm^2/s range of diffusivity values revealed notable discrepancies. Different UTS data points within this range were observed for comparable thermal diffusivity values in the experimental data, while the model would provide an average value. Several factors contribute to this observation.

Firstly, inherent uncertainties in the utilised method, encompassing test and analysis parameters, introduce an uncertainty of around 2.5 %.

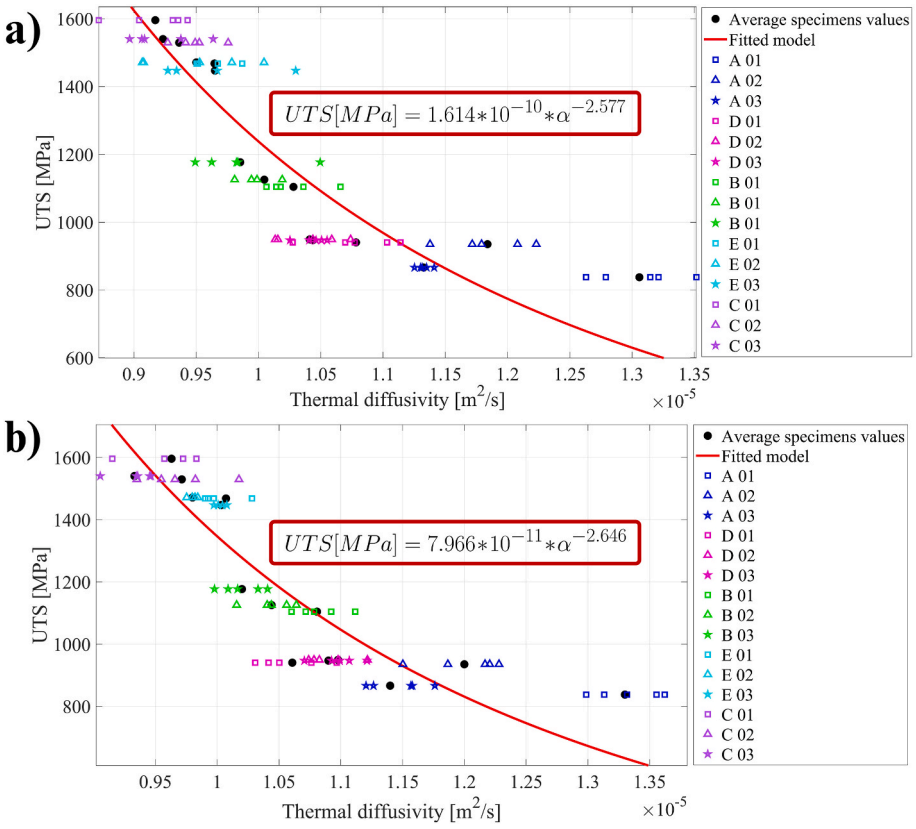

Fig. 11. The Ultimate Tensile Strength (UTS) values for each measurement plotted against the corresponding thermal diffusivity values obtained (a) with coating and (b) without coating. Each colour represents an investigated phase percentage. The red data points indicate the power-law regression obtained and displayed in the red inset. (For interpretation of the references to colour in this figure legend, the reader is referred to the Web version of this article.)

Secondly, considering the geometric attributes of the specimens and the fabrication process, even slight deviations in laser spot alignment with the region of uniform microstructure treatment could impact the measurements. This is because the method takes measurements throughout the thickness of the affected volume.

Furthermore, it is crucial to recognise that the maximum difference between the two extreme conditions, 100 % bainite and 100 % martensite, is approximately 23 % when considering average values. This highlights the significance of the technique's resolution in accurately portraying the trend. Additionally, inherent variability in UTS measurements, which leads to relatively higher uncertainty levels, must be considered, despite the repeatability of results across different specimens.

Moreover, we observed considerable variability in the specimens labelled as A that generate an outlier data point, that if removed, potentially drives the R^2 value beyond 0.88.

The derived relationships provide a reliable means to estimate the phase percentage in the Usibor® 1500 component, enabling the verification of surface heat treatments and non-destructive estimation of its mechanical strength. Significantly, these relationships can be adapted to account for the presence of Al–Si coatings commonly encountered in the supplied state. An estimation of mechanical properties, in case of specimens without coating, can be achieved by incorporating a correction that shifts the curve to the right, reflecting higher thermal diffusivity values. This enhanced methodology holds promise for practical applications in assessing component quality, optimizing manufacturing processes and estimate mechanical properties of component in a non-destructive way.

6. Conclusions

This research presents a non-destructive procedure based on pulsed laser thermography for estimating the mechanical properties of high-strength boron steel, explicitly focusing on the Usibor®1500 grade. The procedure relies on establishing correlations between thermophysical properties, microstructural characteristics, and mechanical behaviour.

Through the analysis of thermal diffusivity measurements obtained using thermographic pulsed laser method, experimental tests were carried out on fifteen meticulously prepared specimens using the Gleeble physical simulator. These specimens encompassed a range of five distinct nominal phase percentages; each replicated three times. Tests were performed both with the Al–Si protective coating typically found on the supplied steel sheets and after its removal, enabling the exploration of the relationship between thermal diffusivity, martensite/bainite phase percentages, and ultimate tensile strength. Intriguingly, an inverse correlation between thermal diffusivity and ultimate tensile strength was observed and confirmed by a Spearman correlation index of −0.98.

The results highlight a degree of uncertainty in the measurements for each investigated phase percentage which is about 5 %. However, this uncertainty stems mainly from the measurement technique, the ultimate tensile strength measurements, and the slight difference in thermal diffusivity between the extreme conditions.

Based on these outcomes, an empirical power-law relationship was established to link the measured thermal diffusivity values obtained via laser-pulsed thermography with the ultimate tensile strength of Usibor® 1500 and a power-law regression model has been considered with R^2 values of 0.82 and 0.84, respectively for coated and uncoated specimens. This facilitates the indirect estimation of the material's mechanical properties through the developed non-destructive procedure. Notably, this estimation can be performed regardless of the presence of the Al–Si coating, as typically encountered in the supplied state or after its removal. These findings bear significant implications for assessing

material integrity and optimizing manufacturing processes.

Future planned developments regarding the presented research activity undoubtedly will involve the application of the method to real hot-stamped components to verify the test procedure's applicability in an industrial context. Furthermore, since one of the aspects to be further investigated is the accuracy of the technique, it will be necessary to evaluate other thermographic methodologies for measuring thermal diffusivity to determine if their sensitivity is suitable for the application under consideration.

Funding

This research is funded by the European Union – NextGenerationEU (National Sustainable Mobility Center CN00000023, Italian Ministry of University and Research Decree n. 1033–17/06/2022, Spoke 11 (Innovative Materials and Lightweighting).

CRediT authorship contribution statement

G. Dell'Avvocato: Conceptualization, Formal analysis, Investigation, Methodology, Validation, Visualization, Writing – original draft. **P. Bison:** Software, Writing – review & editing. **M.E. Palmieri:** Investigation, Validation, Visualization, Writing – original draft. **G. Ferrarini:** Data curation, Investigation, Writing – review & editing, Resources. **D. Palumbo:** Methodology, Supervision, Writing – review & editing. **L. Tricarico:** Funding acquisition, Project administration, Resources, Writing – review & editing. **U. Galietti:** Funding acquisition, Project administration, Resources, Supervision.

Declaration of competing interest

The authors declare that they have no known competing financial interests or personal relationships that could have appeared to influence the work reported in this paper.

Data availability

Data will be made available on request.

References

[1] Palmieri ME, Tricarico L. Numerical-experimental study of a tailored press-hardening technology with intermediate pre-cooling to manufacture an automotive component in advanced high strength steel. In: Materials research proceedings, vol. 25. Association of American Publishers; 2023. p. 447–54. https://doi.org/10.21741/9781644902417-55.

[2] Palmieri ME, Galetta FR, Tricarico L. Study of tailored hot stamping process on advanced high-strength steels. Journal of Manufacturing and Materials Processing 2022;6. https://doi.org/10.3390/JMMP6010011.

[3] Oster S, Breese PP, Ulbricht A, Mohr G, Altenburg SJ. A deep learning framework for defect prediction based on thermographic in-situ monitoring in laser powder bed fusion. J Intell Manuf 2023. https://doi.org/10.1007/s10845-023-02117-0.

[4] Klamert V, Schmid-Kietreiber M, Bublin M. A deep learning approach for real time process monitoring and curling defect detection in Selective Laser Sintering by infrared thermography and convolutional neural networks. Procedia CIRP 2022;111:317–20. https://doi.org/10.1016/j.procir.2022.08.030. Elsevier B.V.

[5] Mattera G, Nele L, Paolella D. Monitoring and control the Wire Arc Additive Manufacturing process using artificial intelligence techniques: a review. J Intell Manuf 2023. https://doi.org/10.1007/s10845-023-02085-5.

[6] Alvarez-Restrepo CA, Benitez-Restrepo HD, Tobón LE. Characterization of defects of pulsed thermography inspections by orthogonal polynomial decomposition. NDT E Int 2017;91:9–21. https://doi.org/10.1016/j.ndteint.2017.05.003.

[7] Pech-May NW, Paul A, Ziegler M. Pulse-compression laser thermography using a modified Barker code: enhanced detection of subsurface defects. SPIE-Intl Soc Optical Eng; 2021. p. 17. https://doi.org/10.1117/12.2586078.

[8] Montinaro N, Cerniglia D, Pitarresi G. Laser thermography NDT for the inspection of debonding in titanium based Fibre Metal Laminates. IOP Conf Ser Mater Sci Eng 2021;1038:012045. https://doi.org/10.1088/1757-899x/1038/1/012045.

[9] Vavilov VP, Pawar SS. A novel approach for one-sided thermal nondestructive testing of composites by using infrared thermography. Polym Test 2015;44:224–33. https://doi.org/10.1016/j.polymertesting.2015.04.013.

[10] Vavilov VP, Burleigh DD. Review of pulsed thermal NDT: physical principles, theory and data processing. NDT E Int 2015;73:28–52. https://doi.org/10.1016/j.ndteint.2015.03.003.

[11] Dell'Avvocato G, Gohlke D, Palumbo D, Krankenhagen R, Galietti U. Quantitative evaluation of the welded area in Resistance Projection Welded (RPW) thin joints by pulsed laser thermography. In: Avdelidis NP, Mendioroz A, editors. Thermosense: thermal infrared applications XLIV. SPIE; 2022. p. 26. https://doi.org/10.1117/12.2618806.

[12] Ibarra-Castanedo C, Maldague X. Pulsed phase thermography reviewed. Quant InfraRed Thermogr J 2004;1:47–70. https://doi.org/10.3166/qirt.1.47-70.

[13] Lecompagnon J, Hirsch PD, Rupprecht C, Ziegler M. Nondestructive thermographic detection of internal defects using pixel-pattern based laser excitation and photothermal super resolution reconstruction. Sci Rep 2023;13. https://doi.org/10.1038/s41598-023-30494-2.

[14] Palumbo D, Galietti U. Damage investigation in composite materials by means of new thermal data processing procedures. Strain 2016;52:276–85. https://doi.org/10.1111/str.12179. Blackwell Publishing Ltd.

[15] Sharkeev YP, Vavilov VP, Skrypnyak VA, Legostaeva EV, Eroshenko AY, Belyavskaya OA, et al. Research on the processes of deformation and failure in coarse- and ultrafine-grain states of Zr1–Nb alloys by digital image correlation and infrared thermography. Mater Sci Eng, A 2020;784. https://doi.org/10.1016/j.msea.2020.139203.

[16] Manteghi S, Sarwar A, Fawaz Z, Zdero R, Bougherara H. Mechanical characterization of the static and fatigue compressive properties of a new glass/flax/epoxy composite material using digital image correlation, thermographic stress analysis, and conventional mechanical testing. Mater Sci Eng C 2019;99:940–50. https://doi.org/10.1016/j.msec.2019.02.041.

[17] Feng X, Xue F. Characterization of 3D printed bolts based on digital image correlation and infrared thermography. Mater Des 2020;191. https://doi.org/10.1016/j.matdes.2020.108641.

[18] Palumbo D, De Finis R, Demelio PG, Galietti U. A new rapid thermographic method to assess the fatigue limit in GFRP composites. Compos B Eng 2016;103:60–7. https://doi.org/10.1016/j.compositesb.2016.08.007.

[19] Parker WJ, Jenkins RJ, Butler CP, Abbott GL. Flash method of determining thermal diffusivity, heat capacity, and thermal conductivity. J Appl Phys 1961;32:1679–84. https://doi.org/10.1063/1.1728417.

[20] Nicolaides L, Mandelis A, Beingessner CJ. Physical mechanisms of thermal-diffusivity depth-profile generation in a hardened low-alloy Mn, Si, Cr, Mo steel reconstructed by photothermal radiometry. J Appl Phys 2001;89:7879–84. https://doi.org/10.1063/1.1373698.

[21] Laskar JM, Bagavathiappan S, Sardar M, Jayakumar T, Philip J, Raj B. Measurement of thermal diffusivity of solids using infrared thermography. Mater Lett 2008;62:2740–2. https://doi.org/10.1016/j.matlet.2008.01.045.

[22] Cernuschi F, Russo A, Lorenzoni L, Figari A. In-plane thermal diffusivity evaluation by infrared thermography. Rev Sci Instrum 2001;72:3988–95. https://doi.org/10.1063/1.1400151.

[23] Mendioroz A, Colom M, Salazar A. Assessing the thermal diffusivity and principal directions of moving samples by infrared thermography: towards fiber orientation monitoring in production chains. SPIE-Intl Soc Optical Eng; 2022. p. 36. https://doi.org/10.1117/12.2618278.

[24] Salazar A, Colom M, Mendioroz A. Laser-spot step-heating thermography to measure the thermal diffusivity of solids. Int J Therm Sci 2021;170. https://doi.org/10.1016/j.ijthermalsci.2021.107124.

[25] Colom M, Bedoya A, Mendioroz A, Salazar A. Measuring the in-plane thermal diffusivity of moving samples using laser spot lock-in thermography. Int J Therm Sci 2020;151. https://doi.org/10.1016/j.ijthermalsci.2020.106277.

[26] Pech-May NW, Mendioroz A, Salazar A. Simultaneous measurement of the in-plane and in-depth thermal diffusivity of solids using pulsed infrared thermography with focused illumination. NDT E Int 2016;77:28–34. https://doi.org/10.1016/j.ndteint.2015.10.001.

[27] Krapez JC, Spagnolo L, Frieß M, Maier HP, ünter Neuer G. Measurement of in-plane diffusivity in non-homogeneous slabs by applying flash thermography. Int J Therm Sci 2004;43:967–77. https://doi.org/10.1016/j.ijthermalsci.2004.02.003.

[28] Bedoya A, González J, Rodríguez-Aseguinolaza J, Mendioroz A, Sommier A, Batsale JC, et al. Measurement of in-plane thermal diffusivity of solids moving at constant velocity using laser spot infrared thermography. Measurement 2019;134:519–26. https://doi.org/10.1016/j.measurement.2018.11.013.

[29] Aouali A, Chevalier S, Sommier A, Pradere C. Terahertz constant velocity flying spot for 3D tomographic imaging. J Imaging 2023;9:112. https://doi.org/10.3390/jimaging9060112.

[30] Bison P, Cernuschi F, Capelli S. A thermographic technique for the simultaneous estimation of in-plane and in-depth thermal diffusivities of TBCs. Surf Coat Technol 2011;205:3128–33. https://doi.org/10.1016/j.surfcoat.2010.11.013.

[31] Bison P, Cernuschi F, Grinzato E. In-depth and in-plane thermal diffusivity measurements of thermal barrier coatings by IR camera: evaluation of ageing. Int J Thermophys 2008;29:2149–61. https://doi.org/10.1007/s10765-008-0421-1.

[32] Qu H, Wang C, Guo X, Mandelis A. Reconstruction of depth profiles of thermal conductivity of case hardened steels using a three-dimensional photothermal technique. J Appl Phys 2008;104. https://doi.org/10.1063/1.3035831.

[33] Wu E, Gao Q, Li M, Shi Y, Mandelis A. Study on in-plane thermal conduction of woven carbon fiber reinforced polymer by infrared thermography. NDT E Int 2018;94:56–61. https://doi.org/10.1016/j.ndteint.2017.11.007.

[34] Krapez J-C, Voti RL. Effusivity depth profiling from pulsed radiometry data: comparison of different reconstruction algorithms. n.d.

[35] Barlow LD, Du Toit M. Effect of austenitizing heat treatment on the microstructure and hardness of martensitic stainless steel AISI 420. J Mater Eng Perform 2012;21:1327–36. https://doi.org/10.1007/s11665-011-0043-9.
[36] Giri LI, Tuli S, Sharma M, Bugnon P, Berger H, Magrez A. Thermal diffusivity measurements of templated nanocomposite using infrared thermography. Mater Lett 2014;115:106–8. https://doi.org/10.1016/j.matlet.2013.10.042.
[37] Ospina-Barras JE, Florez-Ospina JF, Benitez-Restrepo HD, Maldague X. Thermal diffusivity estimation with quantitative pulsed phase thermography. Thermosense: Thermal Infrared Applications XXXVII 2015;9485:948512. https://doi.org/10.1117/12.2178886. SPIE.
[38] Nolte PW, Malvisalo T, Wagner F, Schweizer S. Thermal diffusivity of metals determined by lock-in thermography. Quant InfraRed Thermogr J 2017;14:218–25. https://doi.org/10.1080/17686733.2017.1329777.
[39] Boué C, Holé S. Infrared thermography protocol for simple measurements of thermal diffusivity and conductivity. Infrared Phys Technol 2012;55:376–9. https://doi.org/10.1016/j.infrared.2012.02.002.
[40] Addepalli S, Zhao Y, Erkoyuncu JA, Roy R. Quantifying uncertainty in pulsed thermographic inspection by analysing the thermal diffusivity measurements of metals and composites. Sensors 2021:21. https://doi.org/10.3390/s21165480.
[41] Shepard SM, Lhota JR, Ahmed T, Rubadeux BA, Wang D. Quantification and automation of pulsed thermographic NDE. 2001.
[42] Krapez J-C. Diffusivity measurement by using a grid-like mask Modeling of the infrared remote sensing signal View project LEAK DETECTION IN WATER TRANSMISSION SYSTEMS BY MULTISPECTRAL REMOTE SENSING WITH AIRPLANE AND UAV View project Diffusivity measurement by using a grid-like mask. 2017.
[43] Fudym O, Battaglia JL, Batsale JC. Measurement of thermophysical properties in semi-infinite media by random heating and fractional model identification. Rev Sci Instrum 2005;76. https://doi.org/10.1063/1.1877012.
[44] Pradere C, Caumes JP, Balageas D, Salort S, Abraham E, Chassagne B, et al. Photothermal converters for quantitative 2D and 3D real-time TeraHertz imaging. Quant InfraRed Thermogr J 2010;7:217–35. https://doi.org/10.3166/qirt.7.217-235.
[45] Cernuschi F, Bison P, Marinetti S, Campagnoli E. Thermal diffusivity measurement by thermographic technique for the non-destructive integrity assessment of TBCs coupons. Surf Coat Technol 2010;205:498–505. https://doi.org/10.1016/j.surfcoat.2010.07.024.
[46] Dell'Avvocato G, Palumbo D, Galietti U. A non-destructive thermographic procedure for the evaluation of heat treatment in Usibor®1500 through the thermal diffusivity measurement. NDT E Int 2023:133. https://doi.org/10.1016/j.ndteint.2022.102748.
[47] Dell'Avvocato G, Palumbo D, Palmieri ME, Tricarico L, Galietti U. A non-destructive thermographic procedure for the estimation of mechanical properties in steel through thermal diffusivity measurements. In: Avdelidis NP, editor. Thermosense: thermal infrared applications XLV. SPIE; 2023. p. 14. https://doi.org/10.1117/12.2664838.
[48] Dell'Avvocato G, Palumbo D, Palmieri ME, Galietti U. Non-destructive thermographic method for the assessment of heat treatment in boron steel. SPIE-Intl Soc Optical Eng; 2022. p. 8. https://doi.org/10.1117/12.2618810.
[49] Palmieri ME, Posa P, Angelastro A, Bassan D, Colosseo M, Tricarico L. Analysis of transition zone on a hot-stamped part with tailored tool tempering approach by numerical and physical simulation. Steel Res Int 2023;94. https://doi.org/10.1002/srin.202200665.
[50] Palmieri ME, Tricarico L. Influence of conformal cooling channel parameters on hot stamping tool and press-hardening process. Key Eng Mater 2022;926 KEM:645–54. https://doi.org/10.4028/p-5kczh8. Trans Tech Publications Ltd.
[51] Gustafsson SE. Transient plane source techniques for thermal conductivity and thermal diffusivity measurements of solid materials. Rev Sci Instrum 1991;62:797–804. https://doi.org/10.1063/1.1142087.